 CMC, vol.29, no.2, pp.155-168, 2012

Penetration Analysis of Concrete Plate by 3D FE-SPH Adaptive Coupling Algorithm

D. A. Hu[1,2,3], C. Liang[1], X. Han[1], Y. Z. Chen[4] and W. F. Xu[4]

Abstract: Penetration process of concrete plate is simulated by 3D FE-SPH adaptive coupling algorithm, which is based on experimental research of projectile with 25mm diameter penetrates concrete target. In experiment, a high speed camera is used to record dynamic deformation process of concrete plate. Acceleration responses of concrete are obtained by acceleration sensor, which is pre-embedded in target plate. This experiment is also simulated by 3D FE-SPH adaptive coupling algorithm to verify the numerical model. Numerical model is approximated initially by FEM, and distorted elements are automatically converted into meshless particles to simulate damage, splash of concrete by SPH method, when equivalent plastic strain of elements reaches a specified value. Numerical results of damage process and acceleration response of concrete target are in good agreement with the experimental results. And the results show that crack propagation and lateral movement of concrete mainly occur after projectile passing through target. Furthermore, six different models with different geometry sizes are simulated by the coupling algorithm to study on the effects of boundary condition of concrete target.

Keywords: Penetration, Concrete, Experimental research, FE-SPH coupling algorithm

1 Introduction

Previous researches on experiment and numerical simulation of penetration of concrete target pay more attention to depth of penetration, final damage effects of tar-

[1] State Key Laboratory of Advanced Design and Manufacturing for Vehicle Body, Hunan University, Changsha 410082, P. R. China

[2] State Key Laboratory of Explosion Science and Technology, Beijing Institute of Technology, Beijing 10081, P.R. China

[3] Corresponding author Tel: +86-731-88822325; Fax: +86-731-88823945. E-mail address: hudean@hnu.edu.cn

[4] Institute of Systems Engineering, China Academy of Engineering Physics, Mianyang 621900, P. R. China.

get, residual velocity and deformation of projectile. And few studies have concentrated on acceleration response of concrete target, damage process and other response information in the process of penetration.

Penetration of concrete plate subjected to high velocity impact is often simulated by finite element method (FEM), which has high computational efficiency [Hanchak, Forrestal, Young and Ehrgott (1992); Forrestal, Frew, Hickerson and Rohwer (2003); Frew, Forrestal and Cargile (2006)]. But high velocity impact problems often involve severe deformation of materials, which may lead to extreme element distortions. Removing distortion elements through erosion technique from the model is most likely to cause total energy loss, and accuracy of calculation cannot be guaranteed at the same time. Smoothed particle hydrodynamics (SPH) method [Libersky, Petschek, Carney, Hipp and Allahdadi (1993); Benz and Asphaug (1995)] has an advantage in treating large deformations, and it can naturally simulate damage and splash phenomenon of materials. But its relatively low computational efficiency limits its application in three-dimensional (3D) modeling and analysis.

Therefore, in order to take advantage of both FEM and SPH method, lots of effort had been dedicated to the coupling of SPH and FEM in the past years. Attaway et al. [Attaway, Heinstein and Swegle (1994)] realized the process of SPH coupled with FEM in a program named Pronto by using the master-slave algorithm. De Vuyst et al. [De Vuyst, Vignjevi cand Campbell (2005)] presented a contact algorithm which considered the coupling of meshless point and finite element. Johnson [Johnson (1994)] described techniques that included attachment algorithm, sliding algorithm and automatic generation of particles, which were linked to a standard finite element grid. Fernandez-Mendez et al. [Fernandez-Mendez, Bonet and Huerta (2005)] proposed a method for continuous blending of FEM and SPH, which had been applied in a transient dynamics simulation with severe distortions of elements. Rabczuk et al. [Rabczuk, Rabczuk and Sauer (2006)] summarized coupled algorithm of SPH and FEM in order to find its advantages and disadvantages. Johnson et al. [Johnson, Stryk, Beissel and Holmquist (2002); Johnson and Stryk (2003)] presented 2D and 3D lagrangian algorithm to automatically convert distorted elements into messless particles during dynamic deformation, and also provided contact and sliding algorithms to link particles to elements. Xiao et al. [Xiao, Han and Hu (2011)] presented an alternative coupling algorithm to fulfill calculations of FEM and SPH, and proposed an adaptive coupling technique to improve computational accuracy.

In this paper, based on the experiment of a 25mm diameter projectile penetrating concrete target, several numerical models are established by 3D FE-SPH adaptive coupling algorithm, which is based on the works of Johnson et al. [Johnson, Stryk,

Beissel and Holmquist (2002); Johnson and Stryk (2003)], and Xiao et al. [Xiao, Han and Hu (2011)]. And study mainly focuses on penetration process, target's acceleration response and damage of concrete target influenced by lateral boundary. It's hoped that damage mechanism of concrete plate subjected to high velocity impact can be further recognized by the analysis of experiment and simulation.

2 FE-SPH adaptive coupling algorithm

In order to take advantage of FEM and SPH method, a 3D explicit Lagrangian program to automatically convert distorted elements into meshless particles during the course of calculation has been developed by Johnson and Stryk [Johnson and Stryk (2003)]. In this technique, the initial model can totally consist of elements. An element is converted to a particle when the equivalent plastic strain of element exceeds a specified value (in the range of 0.3–0.6). Criteria other than plastic strain could also be used. All of the element variables, such as stress, strain, internal energy, damage, etc., are transferred to variables of particle. Mass, velocity and center of gravity of meshless particle are set up as those of replaced element. And velocity of particle is obtained from momentum equation of the element. The meshless particle diameters d are determined by $d = \sqrt[3]{V}$, where V is volume of replaced element.

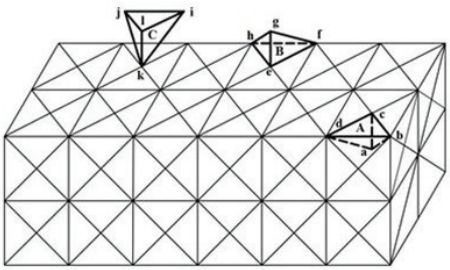

Figure 1: Elements before conversion

Fig. 1 shows a discrete grid with three elements A, B and C on surface, which are designated as candidates for conversion into particles. Fig. 2 shows elements and particles after conversion. Particle A that is generated from element A must be attached to principal plane a-c-d that has the greatest area, and this attachment condition does not allow the particle to slide along or separate from the designated attached plane a-c-d. For the conversion of element B into particle B, generated particle B is designated to be attached to the only remaining master triangle e-f-h, and the attached nodes does not allow it to slide along or separate from triangle

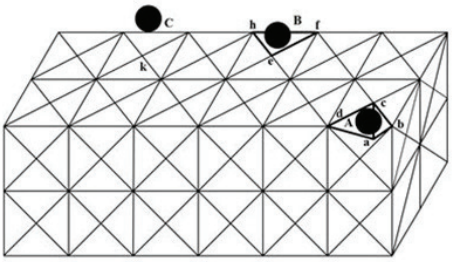

Figure 2: Elements and particles after conversion

e-f-h. The conversion of element C into particle C follows in a similar manner, where all four master triangles are removed and none are added to the list of master triangles. So contact algorithm is used to prevent non-physical penetration.

Papers [Johnson, Stryk, Beissel and Holmquist (2002); Johnson and Stryk (2003); Xiao, Han and Hu (2011)] have much content of FE-SPH adaptive coupling algorithm. In this paper, calculation codes are programmed based on theories of 3D coupling algorithm, and are used to simulate penetration of concrete plate.

3 Establishment of model

Numerical analysis model should be equivalent to penetration experiment model. In the experiment, the target is concrete plate with dimensions of 400mm $\times$ 400mm $\times$ 150mm, compressive strength of 18.5MPa, and tensile strength of 3MPa. The projectile with diameter of 25mm, impacts target with velocity of 510m/s. And material of projectile is 45 steel. Its density and mass is 7.823 g/cm^3 and 230g, respectively. The ratio of projectile diameter to target thickness is 1:6, and ratio of projectile diameter to target length is 1:16.

The layout of experiment and position of acceleration test point are shown in Fig. 3 and Fig. 4. The emission device of experiment is 25mm guns. After passing through concrete plate, the projectile comes into recycling box. In the process of penetration, projectile's flight attitude and damage process of concrete plate can be recorded with a high speed camera. In coordinate $X$and Z direction, as show in Fig. 4, acceleration of point S can be acquired by acceleration sensor, which is pre-embedded in target plate. The distance between test point S and target center is 100mm.

Fig. 5 shows the experimental projectiles, in which the left two are projectiles after experiment and the third one is projectile before experiment. By comparison of

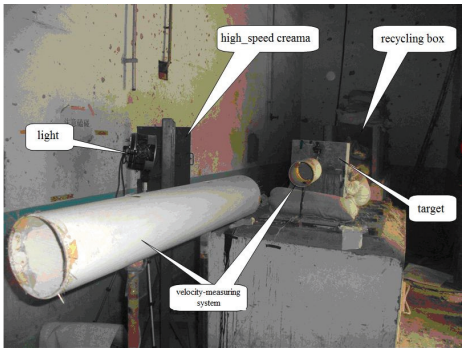

Figure 3: Layout of experiment

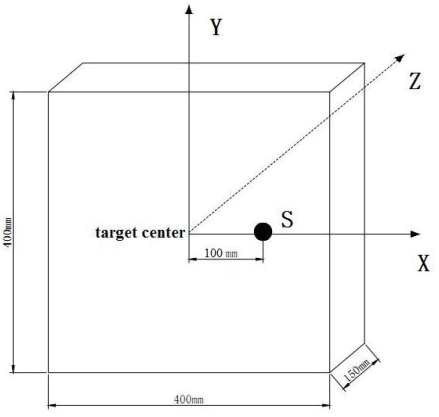

Figure 4: Location of acceleration test point

projectiles before and after experiment, it can be found that projectiles after penetration experiment show only a little abrasion without any deformation. So a rigid projectile model is established in numerical calculation.

Fig. 6 shows 3D numerical analysis model of half experimental model, which is established by using condition of symmetry. The whole model is meshed initially by tetrahedral element. The total number of tetrahedral elements is 363984 in this model. The projectile is modeled with 6480 elements, and concrete plate contains 357504 elements. Lateral surfaces of concrete plate are defined as free boundary, which means considering effect of shock wave reflection. Elements are converted into meshless particles at equivalent plastic strain of ε_p=0.4.

Figure 5: Experimental projectiles

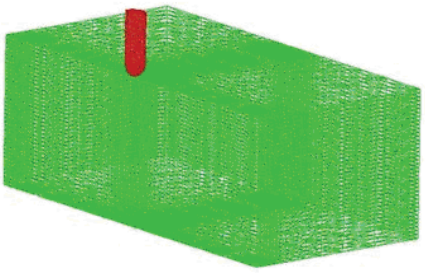

Figure 6: 3D numerical analysis model

To describe large strain, high strain rate, nonlinear deformation and damage of concrete material, Holmquist-Johnson-Cook (HJC) constitutive equation and damage model [Holmquist, Johnson and Cook (1993)] are adopted in numerical analysis. In HJC model, uni-axial compressive strength of f_c=18.5MPa, modulus of elasticity E=34 GPa and tensile strength f_t=3MPa are acquired by test of concrete sample. And the other parameters of HJC model are adopted from Holmquist et al. [Holmquist, Johnson and Cook (1993)].

4 Results analyses

4.1 Applicability analysis of algorithm

The model of projectile penetrating into concrete target is calculated by FE-SPH adaptive coupling algorithm and FEM with erosion technique in LS_DYNA software, respectively. The terminate computation time of both algorithms is 1ms. And 32387 particles are converted from distortion elements in the process of calculation by FE-SPH adaptive coupling algorithm.

Fig. 7 and Tab. 1 show curve of total energy as time changes and loss of total energy calculated by coupling algorithm and FEM with erosion technique, respectively. The finial total energy in Tab. 1 is calculated at the terminate computation time of 1ms. It can be seen that the proportion of energy loss calculated by FE-SPH adaptive coupling algorithm is 9.06% of initial energy, while the energy loss computed by LS_DYNA software takes up about 57.8% of initial energy. Elements of concrete absorbs part of internal energy through elastic and plastic deformation, and a certain kinetic energy is obtained surrounding medium of trajectory of projectile, which is induced by motion of expansion during penetration process. Great loss of total energy is caused by removing distorted elements to avoid abnormal calculation termination in FEM with erosion technique. However, distorted elements will be converted into meshless particles in FE-SPH adaptive coupling method, and their variables are transferred into meshless particle, including stress, strain, mass and internal energy, etc. Then conservation of total energy is basically ensured in calculation by coupling algorithm.

Table 1: Comparison of energy calculated by different algorithms

Item	Initial total energy	Final kinetic energy	Final internal energy	Final total energy	The loss of the total energy	The proportion of the energy loss
LS_DYNA	14.8877	3.8446	2.4403	6.2848	8.6029	57.8%
FE-SPH	14.8877	4.9870	8.5514	13.5384	1.3493	9.06%

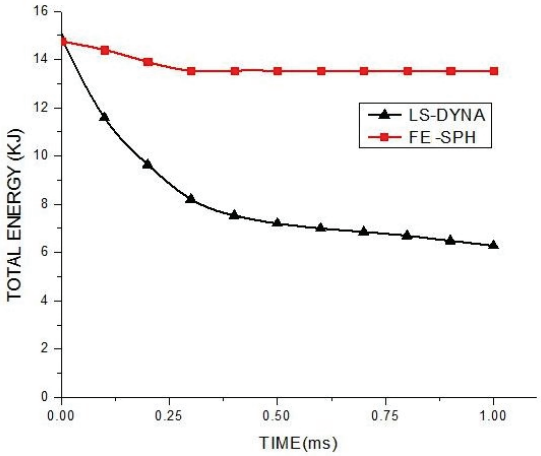

Figure 7: Curve of total energy obtained by different algorithms

4.2 Penetration process of concrete plate

Deformation and damage process of projectile penetrating into concrete plate is effectively presented by 3D FE-SPH adaptive coupling algorithm and experimental high-speed camera, respectively. The penetration process is used to analyze damage mechanism of concrete plate subjected to high velocity impact.

Fig. 8 shows the projectile's deceleration curve in coordinate Z direction, which is obtained by numerical simulation. The deceleration of projectile is induced by resistance force in the process of penetration. In Fig. 8, set up the moment, when projectile begins to contact concrete plate, as the initial time. During time of 0-0.1ms, resistance force of projectile quickly reaches to maximum value due to rapid increasing of contact area between projectile and target plate. This time interval corresponds to making crater stage of penetration process, as show in Fig. 9.

The penetration gets into stable penetration stage during time of 0.1-0.4ms, and projectile has completely entered into target plate at this time. Resistance force gradually decreases as the penetration velocity of projectile reducing. Fig. 10 shows deformation and damage of concrete target that have been obtained by experimental and numerical simulation at time 0.4ms. As shown in Fig. 10, cracks can be clearly observed on lateral surface of target with numerical simulation and experiment. And the time 0.4ms of cracks generating, splashing phenomena of particles calculated by FE-SPH adaptive coupling method are in good agreement with results that recorded by high-speed camera in experiment.

During time of 0.4ms-0.6ms, the penetration enters the stage of passing through

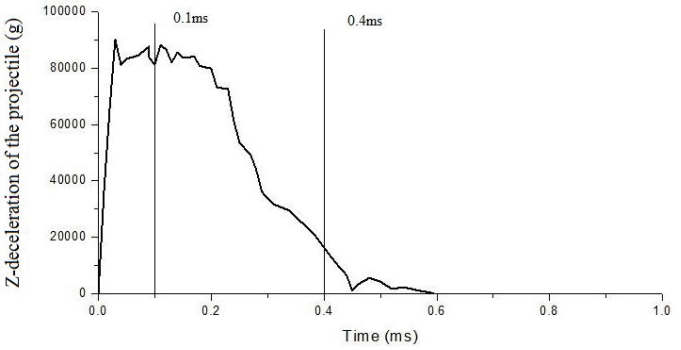

Figure 8: Z-deceleration of projectile

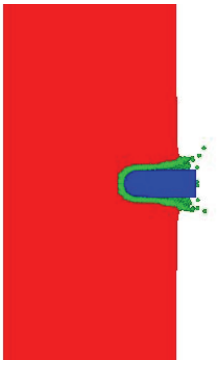

Figure 9: Deformation of target at time 0.1ms

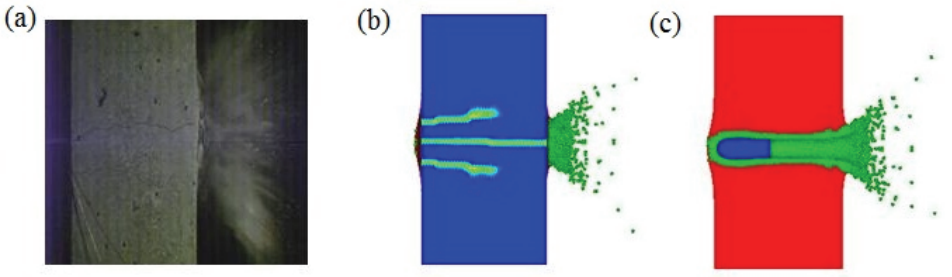

Figure 10: Deformation and damage of target at time 0.4ms (a) Lateral surface of target by experiment (b) Lateral surface of target by numerical simulation (c) Symmetrical surface of target by numerical simulation

target, and resistance force of projectile gradually reduces to zero. At time 0.6ms, the projectile has completely been out of concrete target. Fig. 11 shows deformation of concrete plate with numerical simulation at time 0.6ms. The projectile passes through target as residual velocity is 270m/s.

Fig. 12 shows the deformation and damage of target at time 1.0ms, which are obtained by experimental and numerical simulation. The projectile has been completely away from target plate. Under influences of inertial effect and reflected wave of free boundary, crack propagation and lateral movement of concrete mainly occur after projectile has passed through target.

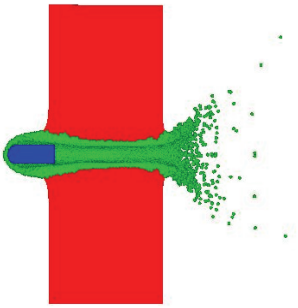

Figure 11: Deformation of target at time 0.6ms

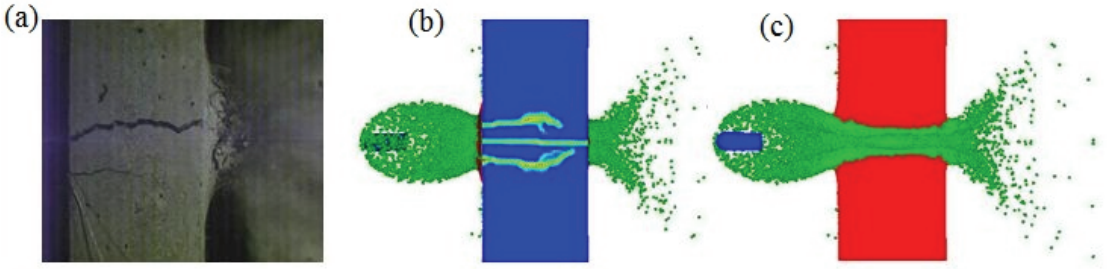

Figure 12: Deformation and damage of target at time 1.0ms (a) Lateral surface of target by experiment (b) Lateral surface of target by numerical simulation (c) Symmetrical surface of target by numerical simulation

4.3 Analysis of acceleration response

Fig. 13 and Fig. 14 show acceleration curves obtained by numerical simulation and experiment at point S in concrete plate. Value of acceleration obtained by numerical simulation has a large movement of oscillation in both coordinate X and Z direction during time of 0-0.2ms. And it is almost in accord with acceleration acquired by experiment. This period corresponds to stage of making crater and primary stage of steady penetration process.

As shown in Tab. 2, maximum peak value of acceleration in coordinate Xdirection measured by experiment is 8500g, and peak value of numerical simulation is 7610g. The relative error of peak value in coordinate Xdirection is 10.47%. The maximum peak value of acceleration in coordinate Z direction obtained by experiment and numerical simulation is 3500g and 3741g, respectively, and their relative error is

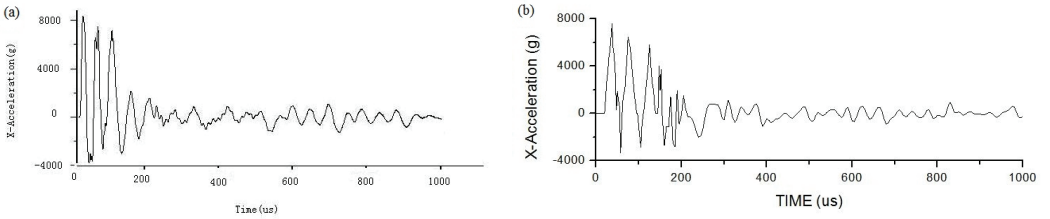

Figure 13: Acceleration curves of point S in coordinate X direction (a) Results of experiment (b) Results of numerical simulation

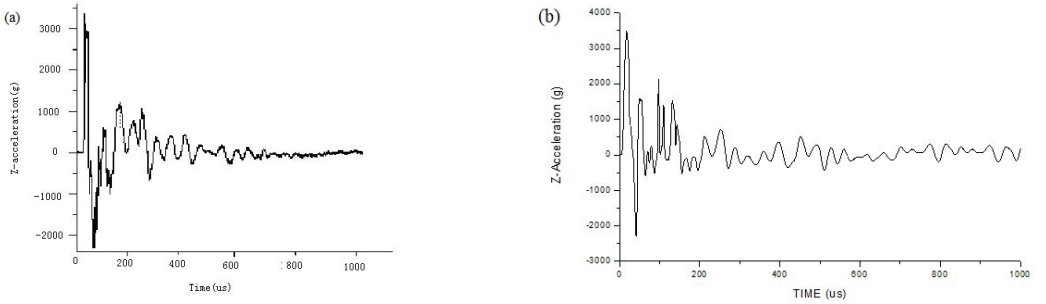

Figure 14: Acceleration curves of point S in coordinate Z direction (a) Results of experiment (b) Results of numerical simulation

6.89%. The above results also demonstrate accuracy of FE-SPH adaptive coupling algorithm in analyzing penetration problems of concrete plate.

Table 2: Comparison of peak value of acceleration at point S

Item	Experimental	Numerical	Relative error
X direction (g)	8500	7610	10.47%
Z direction (g)	3500	3741	6.89%

In addition, acceleration response at point S gradually approaches to zero after time 0.2ms, but crack propagation and lateral movement of concrete almost start at time 0.4ms. This indicates that interaction between projectile and concrete target produces driving force. And the crack propagation and lateral movement of concrete are mainly caused by reflected wave of free boundary, after projectile passing through concrete plate. The peak value of acceleration at point S in coordinate X direction is twice more than that of in coordinate Z direction, which shows that re-

sponse of impact at point S in coordinate X direction (radial direction) is far greater than that of in coordinate Z direction (axial direction). And it indicates that expansion is the main movement of concrete plate in the process of penetration.

5 Penetration analysis of different size targets

As shown by results of experiments and numerical simulations, the boundary condition of concrete target plays a very important influence on deformation and damage process. Then numerical simulation instead of experiment is used to further investigate the influence of boundary condition. And six computational models with different geometry size of concrete plate are established in this paper. The ratio of projectile diameter to targets length of six computational models are 1:8, 1:12, 1:16, 1:20, 1:24 and 1:28 separately. Their corresponding sizes of concrete plate are 20cm×20cm, 30cm×30cm, 40cm×40cm, 50cm×50cm, 60cm×60cm and 70cm×70cm separately. The other geometric and material parameters of projectile and concrete plate are the same with numerical model in section 3 of this paper. And the mesh sizes of numerical simulation remain unchanged in process of calculation for eliminating influence of different mesh.

Tab. 3 shows the loss of projectile's kinetic energy during projectile penetrating through different size targets. The reason is that the closer the distance between lateral boundary of target and center of contact area, the larger intensity of tensile stress wave will occur, which is induced by reflection of shock wave at boundary. The larger intensity of tensile stress wave, the more damage will occur in target, because tensile strength of concrete is much smaller than compression strength. The more damage in target, the smaller resistance force will produce, which is subject to projectile. Therefore, the small target consumes less kinetic energy of projectile in Tab. 3.

Table 3: Kinetic energy loss of projectile

target size(cm)	20×20	30×30	40×40	50×50	60×60	70×70
kinetic energy loss of projectile(KJ)	8.89792	9.21303	9.45468	9.62173	9.80426	10.06424

Fig. 15 shows the damage of different size targets that is subjected to high velocity impact, in which only same regions of 20cm×10cm in center of targets are plotted. It can be seen that as concrete plate size increases, damage area of concrete plate decreases. Fig. 16 shows displacement in coordinate X direction at point A (5cm, 0cm, 0cm) of different size targets. It can be seen from Fig. 16, as the target size increases, the displacement of lateral movement decreases at point A. When the

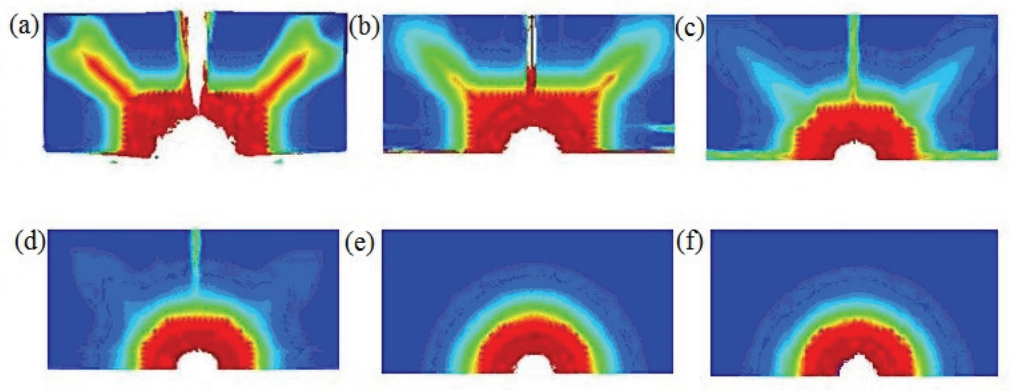

Figure 15: Damage of different size targets (a) 20cm×20cm target (b) 30cm×30cm target (c) 40cm×40cm target (d) 50cm×50cm target (e) 60cm×60cm target (f)70cm×70cm target

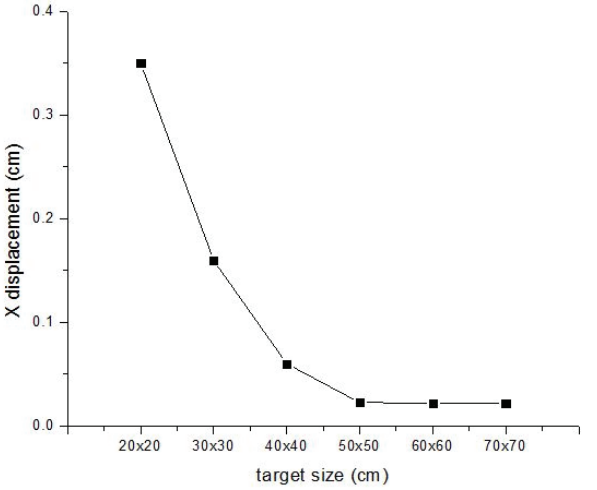

Figure 16: Displacement at point A of different targets

ratio of projectile diameter to target length is 1:20, damage of different size concrete plate is almost consistent, and the X-displacement at point A of different targets is also equivalent with same impact velocity of projectile. It means that influence of boundary condition on penetration damage can be ignored when ration of projectile diameter to target length is 1:20. Actually, the influence of boundary condition could also be estimated from sound speed in concrete, dimension of target and

impact velocity of projectile. Boundary conditions may have little effect if reflected wave arrives at the impact region after projectile leave the target.

6 Conclusion

Based on the experimental researches, the process of projectile penetrating into concrete target has been systematically studied by 3D FE-SPH adaptive coupling algorithm. The results of this paper show that:

(1) The present numerical method has excellent accuracy in analysis of 3D concrete plate penetration problems, and can basically ensure conservation of total system energy. Crater and splash phenomenon of concrete can also be naturally simulated by FE-SPH adaptive coupling method.

(2) The results of experiment and numerical simulation show that projectile penetrating into concrete target contains process of making crater, stable penetration, passing through target, crack propagation, lateral movement of concrete and throwing of fragments. Crack propagation and lateral movement of concrete mainly occur after projectile passing through target.

(3) The targets of different geometry size have been simulated by 3D FE-SPH adaptive coupling algorithm, and the influence of lateral boundary on damage of concrete plate is also analyzed.

Acknowledgement: The financial supports from National Natural Science Foundation of China (10902038) and Open Found of State Key Laboratory of Explosion Science and Technology (KFJJ12-5M) are gratefully acknowledged.

References

Attaway, S.W.; Heinstein, M.W.; Swegle, J.W. (1994): Coupling of Smooth particle hydrodynamics with the finite element method. *Nucl. Eng. Des.*, vol. 150, no. 2-3, pp. 199-205.

Benz, W.; Asphaug, E. (1995): Simulation of brittle solids using smoothed particle hydrodynamics. *Comput. Phys. Commun.*, vol. 87, no. 1-2, pp. 253-265.

De Vuyst, T.; Vignjevic, R.; Campbell, J.C. (2005): Coupling between meshless and finite element methods. *Int. J. Impact Eng.*, vol. 31, no. 8, pp. 1054-1064.

Forrestal, M.J.; Frew, D.J.; Hickerson, J.P.; Rohwer, T.A. (2003): Penetration of concrete targets with deceleration–time measurements. *Int. J. Impact Eng.*, vol. 28, no. 5, pp. 479–497.

Fernandez-Mendez, S.; Bonet, J.; Huerta, A. (2005): Continuous blending of SPH with finite elements. *Comput. Struct.*, vol. 83, no. 17-18, pp. 1448-1458.

Frew, D.J.; Forrestal, M.J.; Cargile, J.D. (2006): The effect of concrete target diameter on projectile deceleration and penetration depth. *Int. J. Impact Eng.*, vol. 32, no. 10, pp. 1584–1594.

Hanchak, S.J.; Forrestal, M.J.; Young, E.R.; Ehrgott, J.Q. (1992): Perforation of concrete slabs with 48 MPa (7 ksi) and 140 MPa (20 ksi) unconfined compressive strengths. *Int. J. Impact Eng.*, vol. 12, no. 1, pp. 1–7.

Holmquist, T. J.; Johnson, G. R.; Cook, W.H. (1993): A computational constitutive model for concrete subjected to large strains, high strain rates, and high pressures. In: Proceedings of 14th international Symposium on Ballistics, Quebec, Canada, pp. 591-600.

Johnson, G.R. (1994): Linking of Lagrangian particle methods to standard finite element methods for high velocity impact computations. *Nucl. Eng. Des.*, vol. 150, no. 2-3, pp. 265-274.

Johnson, G.R.; Stryk, R.A.; Beissel, S.R.; Holmquist, T.J. (2002): An algorithm to automatically convert distorted finite elements into meshless particles during dynamic deformation. *Int. J. Impact Eng.*, vol. 27, pp. 997-1013.

Johnson, G.R.; Stryk, R.A. (2003): Conversion of 3D distorted elements into meshless particles during dynamic deformation. *Int. J. Impact Eng.*, vol. 28, no. 9, pp. 947-966

Libersky, L.D.; Petschek, A.G.; Carney, T.C.; Hipp, J.R.; Allahdadi, F.A. (1993): High strain Lagrangian hydrodynamics: A Three-Dimensional SPH Code for Dynamic Material Response. *J. Comput. Phys.*, vol. 109, no. 1, pp. 67-75.

Rabczuk, T.; Xiao, S.P.; Sauer, M. (2006): Coupling of mesh-free method with finite elements: basic concepts and test results. *Commun. Numer. Meth. En.*, vol. 22, no. 10, pp. 1031-1065.

Xiao, Y.H.; Han, X.; Hu, D.A. (2011): Coupling algorithm of finite element method and smoothed particle hydrodynamics for impact computations. *Comput. Mater. Con.*, vol. 23, pp. 9-34.